CELL BIOLOGY AND METABOLISM:

Endocytosis of Functional Epidermal Growth Factor Receptor-Green Fluorescent Protein Chimera

Royston E. Carter and Alexander Sorkin

J. Biol. Chem. 1998, 273:35000-35007.
doi: 10.1074/jbc.273.52.35000

THE JOURNAL OF BIOLOGICAL CHEMISTRY
Vol. 273, No. 52, Issue of December 25, pp. 35000–35007, 1998

Printed in U.S.A.

Endocytosis of Functional Epidermal Growth Factor Receptor-Green Fluorescent Protein Chimera*

(Received for publication, August 17, 1998, and in revised form, October 7, 1998)

Royston E. Carter and Alexander Sorkin‡

From the Department of Pharmacology, University of Colorado Health Sciences Center, Denver, Colorado 80262

A chimera of the epidermal growth factor receptor (EGFR) and green fluorescent protein (GFP) has been engineered by fusing GFP to the carboxyl terminus of EGFR. Data are provided to demonstrate that the GFP moiety does not affect the expected functioning of EGFR. EGFR-GFP becomes phosphorylated at tyrosine residues in response to EGF and is capable of phosphorylating endogenous substrates and initiating signaling cascades. EGF-dependent association of the chimeric receptor with the clathrin adaptor protein AP-2, involved in endocytosis, and with Shc adaptor protein, which binds in close proximity to the fusion point, is not affected by the GFP moiety. Receptor down-regulation and internalization occur at rates similar to those in cells expressing wild-type EGFR. Western blot analysis reveals that lysosomal degradation of EGFR-GFP proceeds from the extracellular domain and that GFP is not preferentially cleaved. Time-dependent co-localization of EGFR-GFP and Texas Red-conjugated EGF in living cells using digital deconvolution microscopy demonstrates the trafficking of ligand-receptor complexes through the early and multivesicular endosomes followed by segregation of the ligand and receptor at the late stages of endocytosis. Time-lapse optical analysis of the early stages of endocytosis reveals localization of EGFR-GFP in the tubular-vesicular endosomal compartments. Rapid dynamics of membrane movement and fusion within these compartments were observed. This approach and the fidelity of the biochemical properties of the EGFR-GFP demonstrate that real-time visualization of trafficking and protein interactions of tyrosine kinase receptors in the presence or absence of the ligand are feasible.

The endocytosis of epidermal growth factor receptor (EGFR)[1] has served as a model to study the ligand-induced receptor-mediated endocytosis for many years. It is well established that EGF binding to the surface receptors results in down-regulation of EGFR (1, 2). This down-regulation is attributed to the rapid internalization of the activated receptors via clathrin-coated pits followed by the efficient sorting of the internalized receptors to the lysosome degradation pathway (reviewed in Ref. 3).

The mechanism of receptor recruitment into plasma membrane clathrin-coated pits is not well understood. Although EGF-dependent interaction of EGFR with clathrin adaptor complex AP-2 has been demonstrated by several techniques (4–6), the functional significance of this interaction is not formally proven (7, 8). In addition, EGFR can be endocytosed via clathrin-independent pathway. The protein coats involved in this route are not known. Both pathways lead to the same early endosomal compartment (9). These endosomes consist of tubular-vesicular membrane networks where EGF·EGFR complexes are seen co-localized with recycling receptors, for instance, transferrin receptors (10, 11). Both types of receptors are rapidly recycled back to the cell surface from early endosomes (12, 13). However, during continuous endocytosis EGFR become segregated in the vesicular parts of endosomes and subsequently concentrated in multivesicular endosomes (MVE) (12, 14). Once incorporated into internal membranes of MVE, EGFRs are incapable of recycling. MVE can directly fuse with lysosomes (15), which ultimately leads to the proteolytic degradation of EGFR.

To date, visualization of EGFR endocytosis has been largely limited to immunocytochemical analyses on chemically fixed cells. Fixation and following sample preparation for light and electron microscopy analysis often lead to dramatic changes in the morphology of the endosomal compartments and may also cause the artifactual re-distribution of the proteins. Fluorescence microscopy and video recording of living cells using fluorescent conjugates of EGF or antibodies to EGFR have been used to follow the passage of the EGFR through the endosomal compartments (11, 16). However, this approach has major limitations, including non-stoichiometric labeling of the receptors, possible modification of the receptor behavior, partial dissociation of ligand-receptor complexes in acidic organelles and sorting of ligand and receptors to different compartments, and an inability to label intracellular receptors in non-permeabilized cells.

GFP from jellyfish *Aequorea victoria* has been utilized as a reporter molecule in the fluorescent localization of several proteins (17–19). GFP stoichiometrically labels as a fusion protein when integrated into the cDNA and expressed, and it can be excited by blue light and efficiently registered as green fluorescence. However, its size, about 26 kDa, makes it an unlikely candidate for creating a normally functioning EGFR-GFP chimera. Interestingly, we report here the preparation and the characterization of biochemical properties of the functional EGFR chimera with GFP that is fused to the carboxyl terminus of the receptor. The observed behavior of the chimera suggests that EGFR-GFP and other similarly conjugated receptor tyrosine kinases should be important tools *in vivo* for optical measurement of biochemical and biophysical processes relevant to growth factor receptor signaling and trafficking.

* This work was supported by National Institutes of Health Grant DK 46817 and University of Colorado Health Sciences/Howard Hughes Medical Institute Grant (to A. S.) and Cancer League of Colorado Fellowship (to R. E. C.). The costs of publication of this article were defrayed in part by the payment of page charges. This article must therefore be hereby marked "*advertisement*" in accordance with 18 U.S.C. Section 1734 solely to indicate this fact.

‡ To whom correspondence should be addressed: Dept. of Pharmacology, University of Colorado Health Sciences Center, 4200 East Ninth Ave., Denver, CO 80262. Tel.: 303-315-7252; Fax: 303-315-7097; E-mail: alexander.sorkin@uchsc.edu.

[1] The abbreviations used are: EGFR, EGF receptor; GFP, green fluorescent protein; wt, wild-type; EGF, epidermal growth factor; EGF-TR, Texas Red-conjugated EGF; AP-2, clathrin adaptor protein complex; MVE, multi-vesicular endosome; DMEM, Dulbecco's modified Eagle's media; TGH, Triton X-100-glycerol-Hepes buffer; PAE, porcine aortic endothelial; Ab, antibody; PAGE, polyacrylamide gel electrophoresis; MAP, mitogen-activated protein.

MATERIALS AND METHODS

Reagents—Human recombinant EGF was obtained from Collaborative Research Inc. Mouse receptor-grade EGF was iodinated using modified chloramine-T method as described previously (20). The specific activity of ^{125}I-EGF was 1.5–19 × 10^5 cpm/ng. EGF conjugated with Texas Red (EGF-TR) was synthesized using Texas Red *N*-succinimidyl ester (Pierce) according to the manufacturer's protocol. The conjugate (EGF-TR) was purified from free *N*-succinimidyl Texas Red by gel filtration. The binding of EGF-TR to the cells was completely blocked by an excess of unlabeled EGF and is therefore specific.

Polyclonal rabbit antibodies 986 and 451 against EGFR (anti-EGFR) were a gift from Dr. G. Carpenter (Vanderbilt University, Nashville, TN). Rabbit serum Ab2913 specific to the intracellular domain of EGFR was a gift of Dr. L. Beguinot (DIBIT Rafaele, Milan, Italy). Mouse monoclonal antibody 225 hybridoma cells were obtained from ATCC. Mouse monoclonal anti-EGFR (LA22) was purchased from Upstate Biotechnology Inc. Monoclonal antibody to Shc and the anti-phosphotyrosine antibody conjugated with horseradish peroxidase (pY20-HRP) were purchased from Transduction Laboratories. Anti-active MAP kinase was from Promega. Monoclonal and polyclonal antibodies to GFP were from CLONTECH.

Plasmid Construction—A bright green mutant of GFP, enhanced GFP (CLONTECH), was attached to the carboxyl terminus of human EGFR by standard recombinant techniques. Briefly, the full-length cDNA of EGFR including 3′- and 5′-untranslated region sequences was excised from pXER (21) by sequential digestion with *Bgl*II and *Hin*dIII and then ligated into the *Nhe*I and *Hin*dIII sites of pEGFP-N1 (CLONTECH). This yielded a full-length EGFR expression construct that is not fused to GFP, termed pEGFR-wt. To create the EGFR-GFP fusion, this construct was digested with *Hin*cII and *Hin*dIII to remove a fragment containing the distal coding sequence (corresponding to residues 1099–1186 of the coding sequence and the 5′-untranslated region). Then a 492-base pair fragment corresponding to amino acids 1022 and 1186 was prepared by polymerase chain reaction; the back primer contained no stop codon and an engineered *Hin*dIII restriction site. This large fragment was digested with *Hin*cII and *Hin*dIII to yield a replacement fragment of 261 base pairs that was ligated into pEGFR-wt to yield pEGFR-GFP.

Cells—HEK 293 obtained from Dr. D. Cooper (University of Colorado), NIH 3T3, and porcine aortic endothelial (PAE) cells (obtained from Dr. L. Claesson-Welsh, LICR, Uppsala, Sweden) were used for various experiments. HEK 293 and NIH 3T3 cells were maintained in Dulbecco's modified Eagle's medium (DMEM) and PAE cells in Ham's F-12, each containing 10% newborn calf serum, antibiotics, and glutamine in a 5% CO_2 incubator at 37 °C. For most experiments, unless otherwise mentioned, cells were serum-starved overnight in basal media (DMEM or Ham's F-12) supplemented with 5% (v/v) conditioned media.

Transfection—Cells were transfected with pEGFR-GFP or pEGFR-wt DNA using the LipofectAMINE method (Life Technologies, Inc.). Transient transfections were used for all experiments with HEK 293 cells. Stable transformants of NIH 3T3 cells were obtained by selection with G418, and then a pool of bright fluorescent cells was obtained by flow sorting. The sorted pool of EGFR-GFP-expressing cells was maintained and used for experiments as indicated. NIH 3T3 cells expressing wild-type EGFR (wt-1, wt-2, and wt-8) have been described previously (8, 22). Individual clonal lines of NIH 3T3 expressing EGFR-GFP were established by single cell plating into 96-well dishes. PAE cells expressing either EGFR-wt or EGFR-GFP were selected with G418 and established by limited dilution and single cell plating.

Western Blotting—Cells were grown to 50% confluency in various sized culture dishes dictated by the scale of the experiment. The cells were serum-starved overnight. Cells were washed twice with binding media (DMEM or Ham's F-12, 0.1% bovine serum albumin) and then treated or not with EGF in binding media for the times indicated at 37 °C and rinsed twice with ice-cold Ca^{2+},Mg^{2+}-free phosphate-buffered saline (CMF-PBS). Cells were lysed by scraping with a rubber policeman into 100–300 μl of freshly prepared TGH lysis buffer (1% Triton X-100, 10% glycerol, 50 mM Hepes, pH 7.4, with 1 mM orthovanadate, 50 mM NaCl, 5 mM EDTA, 1 mM EGTA, 10 mM sodium fluoride 1 mM phenylmethylsulfonyl fluoride, 10 μg/ml leupeptin, 10 μg/ml iodoacetamide, 10 μg/ml aprotinin, 1% Sigma protease mixture inhibitors). In some instances 1% sodium deoxycholate was added to TGH. Lysates were centrifuged at 14,000 × *g* for 10 min and then mixed with 2× Laemmli buffer and heated at 80 °C for 5 min. Samples were electrophoresed through various concentrations of SDS-PAGE as indicated, and the proteins were transferred to nitrocellulose membranes. Membranes were probed with various monoclonal and polyclonal antibodies which were detected with horseradish peroxidase-labeled secondary antibodies or protein-A and chemiluminescence (Pierce and Amersham Pharmacia Biotech) as described in the figure legends.

Degradation of [^{35}S]Methionine-labeled EGFR-GFP—NIH 3T3 EGFR-GFP cells (clone 11) were grown in 35-mm dishes and metabolically labeled overnight with [^{35}S]methionine (50 μCi per dish) in methionine-free media containing 1% dialyzed calf serum. Cells were washed twice on ice in binding media and then incubated for 30 min in binding media at 37 °C. Cells were rinsed once more in binding media and further incubated with or without 500 ng/ml EGF in binding media for the times indicated. After incubation cells were briefly rinsed in ice-cold CMF-PBS, and the plates were frozen at −80 °C. After all incubations were complete, all cells were thawed and simultaneously scraped into TGH lysis buffer and gently rotated for 10 min as described above. The lysates were centrifuged at 14,000 × *g* for 10 min; the supernatants were recovered, and EGFR was immunoprecipitated with saturating amounts of Ab986 for 3 h at 4 °C, followed by protein-A Sepharose beads for 1 h at 4 °C. The beads were pelleted and washed twice with TGH supplemented with 100 mM NaCl and then once without NaCl. The immunoprecipitates were mixed with Laemmli buffer, heated to 80 °C, and then electrophoresed through an SDS-7.5% polyacrylamide gel. The gel was analyzed by a PhosphorImager (Bio-Rad) and exposed to x-ray film.

Co-immunoprecipitation of AP-2 and Shc—Co-immunoprecipitation of EGFR interacting proteins was performed on NIH 3T3 clones stably expressing EGFR-wt (wt-8) and EGFR-GFP (GFP-11). Cells were plated at 25% confluency in appropriate media and grown overnight. They were then serum-starved overnight in basal media supplemented with 5% conditioned media. Cells were washed twice in binding medium and then incubated with or without 500 ng/ml EGF in binding medium for 8 min at 37 °C. Cells were lysed in TGH buffer as described above. The lysates were centrifuged at 100,000 × *g* for 20 min at 4 °C, and the supernatants were split into two aliquots incubated with Ab451 or normal rabbit IgG for 3 h at 4 °C and then 1 h after addition of protein A-Sepharose. Immunoprecipitates were washed twice with cold TGH supplemented with 100 mM NaCl and then once without NaCl. The electrophoresis, transfer to nitrocellulose membranes, and Western blot analysis were carried out as described above.

Internalization of ^{125}I-EGF—To monitor ^{125}I-EGF internalization, cells in 12-well dishes were incubated with ^{125}I-EGF in binding medium at 37 °C for 1–6 min. The concentration of ^{125}I-EGF was 0.2–1 ng/ml to occupy less than 15,000 receptors per cell and to avoid saturation of the internalization machinery. After the indicated times, the medium was aspirated, and the monolayers were rapidly washed three times with DMEM to remove unbound ligand. The cells were then incubated for 5 min with 0.2 M acetic acid, pH 2.8, containing 0.5 M NaCl at 4 °C. The acid wash was combined with another short rinse in the same buffer and used to determine the amount of surface-bound ^{125}I-EGF. Finally the cells were lysed in 1 M NaOH to determine the internalized radioactivity. The ratio of internalized:surface radioactivity was plotted against time. The linear regression coefficient of the dependence of this ratio for time represents the specific rate constant for internalization. Nonspecific binding was measured for each time point in the presence of 100-fold molar excess of unlabeled EGF and was not more than 3–7% of the total counts.

EGFR Down-regulation—To monitor EGFR down-regulation, cells in 12-well dishes were incubated for various times with or without EGF (100 ng/ml) in binding medium at 37 °C and rinsed with cold DMEM, and surface-bound EGF was removed by successive incubations with ice-cold 0.2 M sodium acetate buffer, pH 4.5, containing 0.5 M NaCl for 2 min and 20 s followed by two rinses with DMEM. The acid wash procedure did not affect the binding properties of EGFR. The number of binding sites on the cell surface was then determined by incubating the cells with 100 ng/ml ^{125}I-EGF at 4 °C for 1 h.

Immunofluorescence Staining in Fixed Cells—Cells grown on coverslips were washed twice in binding media and then treated with EGF. Cells were then washed in CMF-PBS and fixed with freshly prepared 4% paraformaldehyde (Electron Microscopy Sciences) for 12 min at room temperature. Cells were permeabilized with CMF-PBS containing 0.1% Triton X-100, 0.1% bovine serum albumin for 3 min. Coverslips were then incubated in the same buffer, in which Triton X-100 was omitted, at room temperature for 1 h with the primary antibody (Ab225 for EGFR), washed intensively, and then incubated with secondary donkey anti-mouse IgG labeled with Texas Red (ImmunoResearch Laboratories, Inc.). The primary and secondary antibody solutions were precleared by centrifugation at 100,000 × *g* for 10 min. The cells were then mounted in Fluoromount-G (Fisher) containing 1 mg/ml *para*-phenylenediamine. A Nikon Diaphot 300 microscope equipped with ×

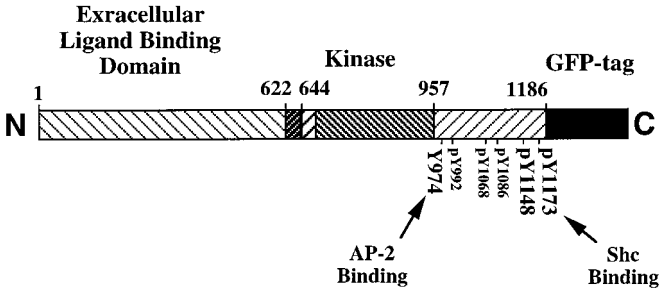

FIG. 1. **Schematic representation of the EGFR-GFP chimera.** The EGFR consists of three major domains as follows: a glycosylated extracellular domain (amino acids 1–622) involved in ligand binding, a single transmembrane domain (amino acids 622–644), and an intracellular domain consisting of a kinase catalytic region (amino acids 663–957) and a carboxyl-terminal region (amino acids 958–1186) which can be phosphorylated at multiple tyrosines (*pY*). The GFP moiety is fused to the carboxyl terminus of EGFR. The position of five major tyrosine phosphorylation sites and the main binding sites of AP-2 (tyrosine 974) and Shc are indicated.

100 1.4 numerical aperture oil immersion objective lens, and the single fluorochrome filter sets for either Texas Red, fluorescein (for GFP), or simultaneous Texas Red/fluorescein fluorescence (Chroma Inc.) were used for visualization and recording the images.

Living Cell Fluorescence Imaging—PAE cells expressing EGFR-GFP (clone A11) were grown in glass chambers (Bioptechs, Inc.), and serum-starved overnight. For double-color time-lapse microscopy, cells were washed once with binding medium, and then the chamber was mounted onto the microscope stage, and the image acquisition through the narrow GFP (excitation 492/10 nm) or Texas Red (excitation 572/10) channels was started. EGF-TR (20 ng/ml) was added to the chamber and washed away after 5 min of incubation. The cells were further incubated in CO_2 incubator at 37 °C and periodically mounted on a microscope stage for image acquisition. Typically, 15–25 serial two-dimensional images were recorded at 200-nm intervals using a thermoelectrically cooled charged-coupled device (CCD) Micromax camera (Princeton Instruments), Nikon Diaphot microscope equipped with z-step motor and dual filter wheel controlled by QED Imaging software. The intensity of light was decreased to 5% of maximum by neutral filters. Image deconvolution was performed on DeltaVision workstation (Applied Precision, Inc.).

To observe rapid dynamics of EGFR-GFP endocytosis, EGF (100 ng/ml) was added to the cell chamber, and GFP images were acquired 2 times per s (0.3-s exposure) continuously during incubation at 37 °C on a microscope stage.

RESULTS

Expression and Turnover of EGFR-GFP—To prepare fluorescent-labeled EGFR, the GFP was fused to the carboxyl terminus of full-length human EGFR (Fig. 1). Carboxyl terminus is a domain that undergoes serine and tyrosine phosphorylation in response to EGF and docks several molecules involved in receptor signaling and trafficking. Placing a 26-kDa protein near this regulatory domain may affect EGFR functioning. Therefore, the properties of the chimeric receptor must be characterized prior to its use in optical microscopy studies.

EGFR-GFP has been expressed both transiently and stably in several cell lines that either possess low levels or lack any detectable endogenous EGFR. Fig. 2 shows Western blot analysis of the stable expression of EGFR-GFP in NIH 3T3 cells that have been previously used in several studies of transfected EGFR. Cells were treated or not treated with EGF, and the lysates were probed with antibodies specific for human EGFR or GFP (Fig. 2, *A* and *B*). Both antibodies reveal the predicted size for the chimera (~203 kDa). Anti-EGFR does not identify free EGFR at 175 kDa, and anti-GFP do not detect free GFP at 26 kDa (data not shown). Together these data confirm the stability of EGFR-GFP.

After prolonged incubation with EGF, three lower molecular weight fragments of EGFR-GFP migrating at approximate molecular mass of 160, 120, and 117 kDa (seen in longer exposures) appear (Fig. 2, *A* and *B*). To determine whether the low molecular weight fragments are the degradation products or newly synthesized immature receptors, NIH 3T3 cells expressing EGFR-GFP were treated with EGF in the presence or absence of chloroquine, a drug that specifically blocks the lysosomal degradation of EGFR. As shown in Fig. 3*A*, in the absence of chloroquine, EGF-dependent degradation of the receptor occurs with the accumulation of 160-, 120-, and 117-kDa bands. In contrast, chloroquine blocks degradation as demonstrated by the increase in levels of full-length receptor (includes newly synthesized receptor) and by the absence of degradation products. Since detection of EGFR-GFP with anti-GFP is dependent upon the intact carboxyl terminus, the initial degradation of EGFR-GFP involves the extracellular domain of the receptor. The inhibition of degradation by chloroquine implicates lysosomal enzymes.

Activation and Phosphorylation of EGFR-GFP—Activation of the EGFR occurs as a consequence of ligand binding leading to receptor dimerization and tyrosine autophosphorylation and is also accompanied by a characteristic gel shift of the receptor band to an apparent higher molecular weight species. As shown in Fig. 2, EGF binding results in appearance of slow-migrating forms of EGFR-GFP indicating normal receptor activation. The EGFR-GFP activation persists for at least 1 h, after which dephosphorylation, characterized by a return to the native molecular weight mobility, is observed. This dephosphorylation is accompanied by down-regulation of the receptor.

Phosphotyrosine immunoblotting demonstrates rapid tyrosine phosphorylation of EGFR-GFP and a number of cellular proteins upon EGF stimulation (Fig. 2*C*). The pattern of phosphorylation/dephosphorylation of cellular proteins in response to EGF was similar to that in cells expressing wild-type EGFR (EGFR-wt), although small qualitative and quantitative differences were observed when various clones of NIH 3T3 cells expressing EGFR-GFP and EGFR-wt were compared. The level of EGFR-GFP and EGFR-wt phosphorylation is gradually decreased over the course of the 6-h experiment with the half-life of approximately 3 h. These data indicate the appropriate signaling capabilities of EGFR-GFP.

Activation of MAP kinase (Erk1/2) is a trademark of EGF-induced signal transduction cascade (23). To test whether EGFR-GFP is capable of mediating MAP kinase activation, lysates of NIH 3T3 cells expressing EGFR-GFP were probed with the antibodies specifically recognizing the activated MAP kinase. Fig. 3*B* demonstrates substantial EGF-dependent activation of Erk1/2, which returns to a basal level within 2–6 h. The extent and time course of MAP kinase stimulation were essentially the same in cells expressing EGFR-GFP and wild-type EGFR (EGFR-wt) (data not shown). In cells treated with chloroquine MAP kinase remains maximally active during at least 6 h, which parallels the activity of EGFR-GFP (Fig. 3*B*).

Protein-Protein Interactions of EGFR-GFP—Experiments presented in Figs. 2 and 3 suggest that the chimeric EGFR-GFP preserves functional activity. The initial EGF-induced events following receptor activation are mediated by interactions of the receptor carboxyl terminus with several proteins. For instance, the Shc adaptor protein (46- and 52 kDa forms) is a major receptor-binding partner *in vivo* involved in signaling of the EGFR (24). The binding of Shc to EGFR requires phosphorylation of tyrosines 1148 and 1173 located near the fusion point in the EGFR-GFP chimera (25). Binding of AP-2 to Tyr-974 is implicated in the regulation of receptor endocytosis (8). The ability of EGFR-GFP to interact with Shc and AP-2 was tested in NIH 3T3 cells using co-immunoprecipitation assay (Fig. 4). Western blot analysis of receptor immunoprecipitates

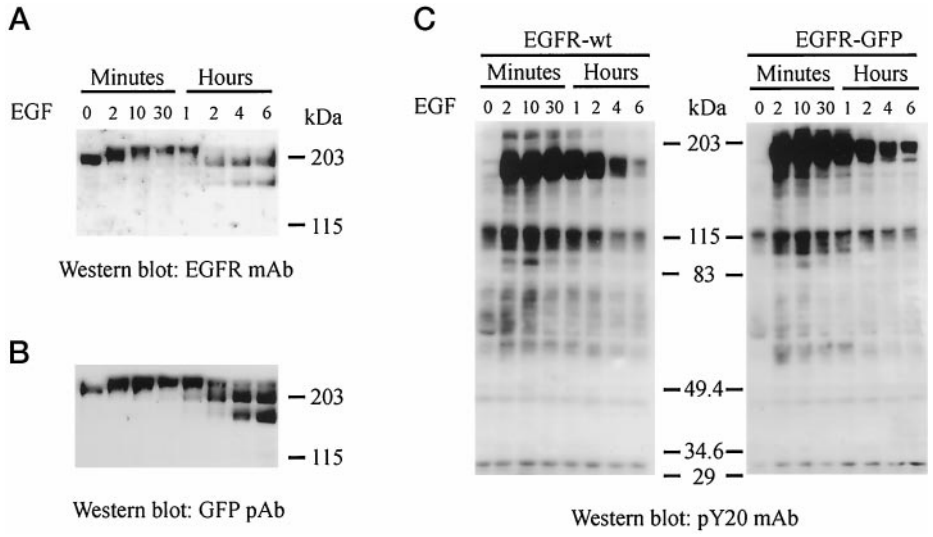

FIG. 2. **Expression of EGFR-GFP in mammalian cells.** NIH 3T3 cells stably transfected with EGFR-GFP (pool of stable transfectants) or EGFR-wt (clone wt-2) were grown in duplicate 12-well dishes to 80% confluency and then serum-starved overnight. Cells were washed and then treated with 500 ng/ml EGF for the times indicated above. Cells were lysed in TGH, and duplicate aliquots were electrophoresed through 6–10% gradient (*A* and *B*) and 7.5% SDS-PAGE and transferred to nitrocellulose membranes. *A*, shows Western blot analysis with anti-EGFR antibody LA22 (EGFR monoclonal antibody (*mAb*)); *B*, shows Western blot analysis with anti-GFP antibodies (GFP polyclonal antibody (*pAb*)) of the same experiment. *C*, shows Western blot analysis with anti-phosphotyrosine antibody (pY20-HRP) of a similar independent experiment.

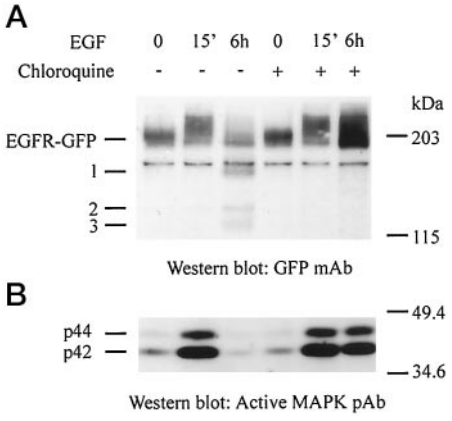

FIG. 3. **Effect of chloroquine on EGFR degradation and activation.** NIH 3T3 cells stably transfected with EGFR-GFP (pool) or EGFR-wt (clone wt-8) were grown in 12-well dishes to 80% confluency and then serum-starved overnight. Cells were treated or not with 500 ng/ml EGF and 200 μM chloroquine and lysed in TGH supplemented with sodium deoxycholate. The lysates were resolved by a 7.5% SDS-PAGE and transferred to nitrocellulose membranes. The *upper* portion of the membrane, *A*, was probed with anti-GFP (GFP monoclonal antibody (*mAb*)). The low molecular weight fragments of EGFR-GFP are labeled *1, 2,* and *3*. The anti-GFP monoclonal antibody detects a prominent nonspecific band ~165 kDa, whose level does not vary under any conditions. This band was not detected with antibody specific for the intracellular domain of EGFR, Ab2913 (data not shown). *B*, shows a *lower* portion of the same membrane probed with anti-active MAP kinase (*MAPK*) antibodies. *pAb*, polyclonal antibody.

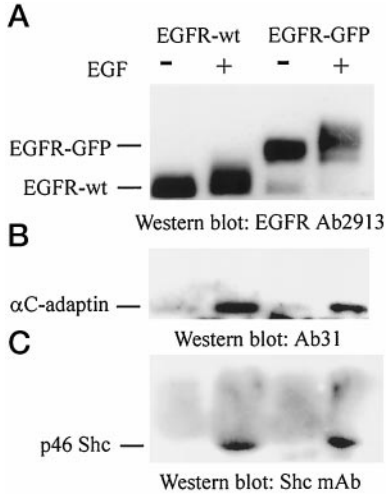

FIG. 4. **Co-immunoprecipitation of AP-2 and Shc with EGFR-wt and EGFR-GFP.** Duplicates of clonal NIH 3T3 cells expressing EGFR-wt (clone wt-8) or EGFR-GFP (clone 11) cells were grown on 100-mm tissue culture plates to about 50% confluency and serum-starved overnight. Cells were incubated or not with 500 ng/ml EGF in binding medium for 8 min at 37 °C. EGFRs were then immunoprecipitated from TGH lysates with anti-EGFR number 451. Normal rabbit IgG fraction was used as nonspecific control. Immunoprecipitates were resolved through a 7.5% SDS-PAGE and transferred to a nitrocellulose membrane. *A*, Western blotting for the precipitated receptors with anti-EGFR Ab2913. *B*, Western blotting of α-C adaptin detected with Ab31. *C* shows Western blotting with anti-Shc antibody. *mAb*, monoclonal antibody.

from EGFR-wt- and EGFR-GFP-expressing cells demonstrate similar levels of EGF-dependent association of α-adaptin, a marker of AP-2 complex, and both Shc p46 and p52 (p52 band obscured by IgG heavy chain, data not shown). These data strongly indicate the similar biochemical properties of the chimeric and native EGFR and together with Figs. 2 and 3 demonstrate that the GFP moiety does not affect the activity of EGFR.

EGF-dependent Receptor Down-regulation—The decrease in the expression level of the receptor (down-regulation) is a characteristic feature of the effect of ligand activation of the EGFR and other receptor tyrosine kinases. Fig. 5*A* demonstrates EGF-dependent down-regulation of the receptor in NIH 3T3 cells expressing different levels of wt-EGFR or EGFR-GFP and in transiently transfected HEK 293 cells. In NIH 3T3 cells the number of EGF-binding sites at the surface in cells expressing EGFR-GFP or EGFR-wt is decreased at similar rates in the presence of EGF. Interestingly, when EGFR-GFP or EGFR-wt were transiently expressed in HEK 293 cells, EGF did not cause significant loss of the surface EGF-binding sites, whereas endogenous receptors in these cells are down-regulated very rapidly (Fig. 5*A*).

To measure specifically the degradation of the receptor protein, NIH 3T3 cells expressing EGFR-GFP were metabolically labeled with [^{35}S]methionine and then treated for up to 4 h with EGF. Receptors were immunoprecipitated from cell lysates with anti-EGFR. As shown in Fig. 5*B*, EGF induces rapid degradation of EGFR-GFP with a half-life time of about 1.5 h. This value is in close agreement with the previously determined values for EGFR-wt expressed in NIH 3T3 cells (8, 20). The products of partial proteolysis of EGFR-GFP (Figs. 2 and 3) were not immunoprecipitated, probably due to a poor recognition of these truncated forms by the antibody 986 specific to the extracellular domain of native EGFR.

Internalization of ^{125}I-EGF—The apparent rates of EGFR down-regulation and degradation are determined by the spe-

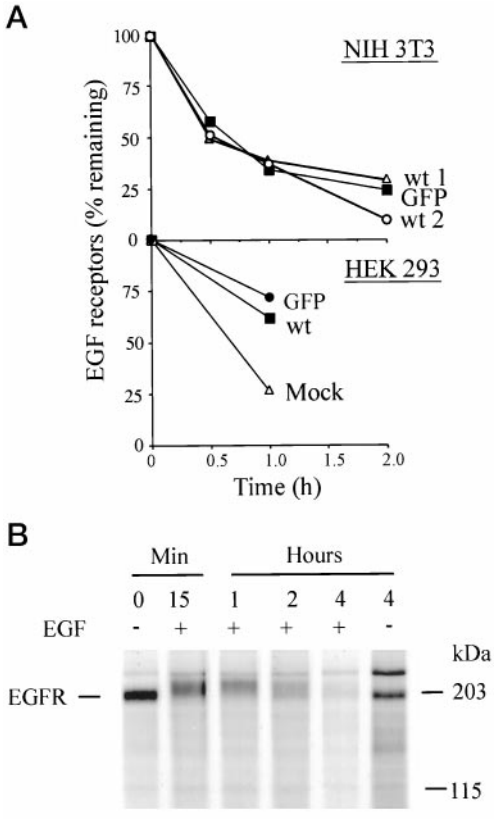

FIG. 5. **Down-regulation and degradation of EGFR.** The time course for down-regulation of receptors was determined for NIH 3T3 cells stably expressing two different levels of EGFR-wt or EGFR-GFP and HEK 293 cells transiently transfected with EGFR-wt or EGFR-GFP. Cells were incubated with 100 ng/ml EGF for the times indicated, and the residual number of surface receptors was determined as described under "Materials and Methods." Binding is expressed as percent of the ^{125}I-EGF binding in EGF-untreated cells. In the *upper panel* of *A*, down-regulation in NIH 3T3 cells expressing EGFR-wt (wt-1, 1×10^5 receptors/cell, *open triangle*; wt-2, 2.5–3.0 $\times$ 10^5 receptors/cell, *open circle*) or EGFR-GFP (clone 11, 1.9×10^5 receptors/cell, *closed square*) are shown. The *lower panel* shows down-regulation in HEK 293 cells (mock transfected, *open triangle*) or transiently overexpressing EGFR-wt (*closed square*) or EGFR-GFP (*closed circle*). *B*, NIH 3T3 cells stably expressing EGFR-GFP (clone 11) were metabolically labeled with [^{35}S]methionine and then treated or not treated with 500 ng/ml EGF at 37 °C in binding medium for the times indicated. EGFR-GFP receptor was immunoprecipitated from the TGH lysate with anti-EGFR Ab986. The immunoprecipitates were resolved on a 7.5% SDS-PAGE, and the gel was dried and exposed to x-ray film.

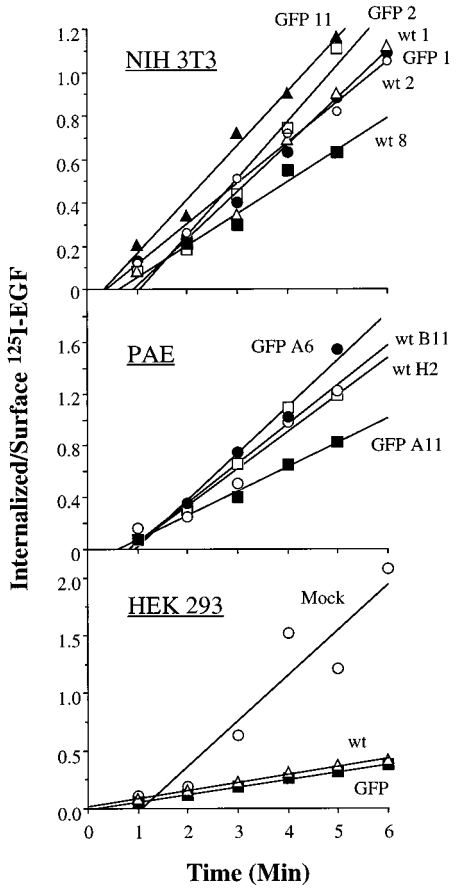

FIG. 6. **Internalization of ^{125}I-EGF by EGFR-wt- and EGFR-GFP-expressing cells.** Cells expressing EGFR-wt or EGFR-GFP were incubated with 0.2–1.0 ng/ml ^{125}I-EGF for 1–6 min, and the amount of surface-bound and internalized radioactivity was determined as described under "Materials and Methods." The rate of internalization is expressed as the ratio of internalized and surface ^{125}I-EGF for each time point. In the *top panel*, NIH 3T3 cells expressing EGFR-wt (wt-1, *open triangle*; wt-2, *open circle*; wt-8, 5–6 $\times$ 10^5 receptors/cell; *closed square*) or EGFR-GFP (GFP 1, *closed circle*; GFP 2, *open square*; GFP 11, *closed triangle*). The *center panel* shows PAE cells stably expressing EGFR-wt (B11, 3.8×10^5 receptors/cell, *open square*; H2, 1.3×10^5 receptors/cell, *open circle*) or EGFR-GFP (A6, 3×10^5 receptors/cell, *closed circle*; A11, 12.7×10^5 receptors/cell, *closed square*). The *bottom panel* shows HEK 293 cells mock-transfected (*open circle*) or transiently overexpressing EGFR-wt (*open triangle*) or EGFR-GFP (*closed square*).

cific rates of several trafficking processes, including internalization, recycling, and lysosomal targeting. Thus, similar kinetics of down-regulation of EGFR-GFP and EGFR-wt suggests that the individual endocytic processes occur at similar speeds for both receptor forms. To compare directly the specific rates of internalization of EGFR-wt and EGFR-GFP via saturable clathrin-dependent pathway, the short time course of ^{125}I-EGF uptake was measured by briefly exposing cells to low levels (1 ng/ml or less) of ^{125}I-EGF at 37 °C. Fig. 6 compares the internalization velocities among different NIH 3T3, PAE, and HEK 293 cells expressing EGFR-GFP or EGFR-wt. NIH 3T3 cells expressing EGFR-wt or EGFR-GFP internalize ^{125}I-EGF at similar rates. Cells, which express high levels, tend to internalize ^{125}I-EGF more slowly, probably due to saturation of the internalization pathway.

The endocytic behavior of EGFR is well studied in transfected NIH 3T3 cells, and these cells have been, therefore, used for initial comparison of EGFR-GFP and EGFR-wt. However, NIH 3T3 cells express endogenous receptors and show substantial autofluorescence that interferes with the visualization of GFP. Thus, we have also chosen to express EGFR-GFP in a new cell line, porcine aortic endothelial (PAE) cells, in which the endogenous EGFR is undetectable by biochemical methods. PAE cells are easy to transfect and have a morphology that is convenient for optical studies. These cells were previously used for expression of platelet-derived growth factor receptors (26), and therefore, the signal transduction cascades are studied reasonably well in this cell line.

The *middle panel* shows a comparison between the rate of internalization of ^{125}I-EGF among two PAE clones stably expressing EGFR-wt (clones B11 and H2) and two that express EGFR-GFP (clones A11 and A6). In general, ^{125}I-EGF internalization occurs at a similar rate in PAE cells expressing EGFR-wt or EGFR-GFP. EGFR-GFP clone A11 displays somewhat slower kinetics of internalization, presumably due to its high level of receptor expression. The specific rates of EGF internalization (Fig. 6) and down-regulation (data not shown) in PAE cells are well within the range of these rates in other cell types. These results validate the use of PAE cells expressing EGFR-GFP in studies of endocytosis of the EGFR.

Interestingly, when the internalization of ^{125}I-EGF was

measured in HEK 293 cells that were transiently transfected with EGFR-wt or EGFR-GFP, the rates of endocytosis were very low. In contrast, the internalization of EGF in mock-transfected HEK 293 cells that express about 20,000 endogenous receptors per cell was very rapid. This result is consistent with an inefficient EGF-induced down-regulation of EGFR in these cells (Fig. 5*A*). Therefore, the endocytic machinery in HEK 293 cells has a very low capacity for EGFR and is saturated by the large number of transfected EGFR regardless of their occupancy by EGF.

Co-localization of GFP and EGFR—The endocytosis of EGFR-GFP expressed in PAE cells can be readily visualized by fluorescence of GFP. GFP localization in the cells incubated with EGF for 30 min at 37 °C and then formaldehyde-fixed is shown in Fig. 7*a*. The punctate staining of EGFR-GFP is seen at the periphery and in the perinuclear regions of the cell, which probably correspond to endosomal compartments. GFP is also accumulated in the Golgi apparatus area, which is likely to represent endosomal as well as newly synthesized EGFR-GFP. The pattern of staining of the cells with anti-EGFR is identical to that of EGFR-GFP, although the intensity of fluorescence is higher due to enhancement of the signal in indirect immunofluorescence staining (Fig. 7*b*). This result supports the Western blot analysis (Fig. 2) suggesting that no significant amounts of free EGFR or GFP are present in EGFR-GFP-expressing cells. PAE cells expressing EGFR-wt show a similar distribution of EGFR immunoreactivity (Fig. 7*d*), whereas no green fluorescence is detected (Fig. 7*c*), indicating the specificity of the detection of GFP fluorescence in our microscope system.

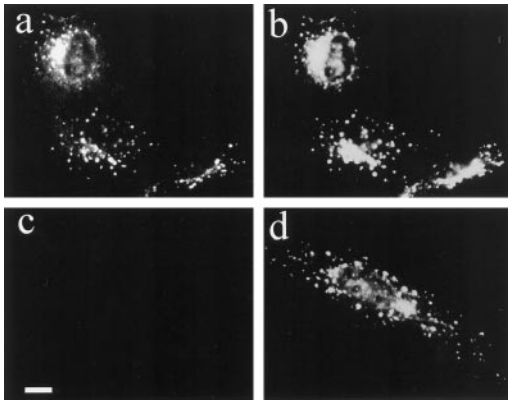

FIG. 7. **Co-localization of GFP and receptor.** PAE cells expressing EGFR-wt (clone B11) (*c* and *d*) or EGFR-GFP (clone A11) (*a* and *b*) were incubated with EGF (200 ng/ml) at 37 °C for 30 min. Cells were fixed and permeabilized briefly in X-100 buffer and then incubated with anti-EGFR (Ab225) followed by the secondary antibodies conjugated with Texas Red. Texas Red (*b* and *d*) and GFP fluorescence (*a* and *c*) are visualized using conventional epifluorescence microscopy. *Bar*, 5 μm.

Endocytosis of EGFR-GFP in Living Cells—The characterization of stable expression of EGFR-GFP described above suggests that this chimera is indeed an appropriate tool to study EGFR trafficking using optical microscopy of living cells. In following experiments the EGF-induced endocytosis of EGFR-GFP was visualized in PAE cells. An important question that could now be addressed was to compare the postendocytic localization of the ligand, EGF, and the EGFR. Cells were allowed to internalize EGF-TR at 37 °C, and the time course of cellular distribution of green and red fluorescence was monitored in living cells using QED Imaging system. The binding of EGF-TR and its diffuse staining on the cell surface is clearly seen after 1 min of EGF-TR addition (Fig. 8, *a–c*). Cells were allowed to internalize further EGF-TR for 4 min, washed to remove unbound ligand, and chased at 37 °C in binding media without ligand. The images of GFP and Texas Red fluorescence were acquired following additional 20–30 and 60–70 min of continuous endocytosis at 37 °C. As shown in Fig. 8, *d–f*,

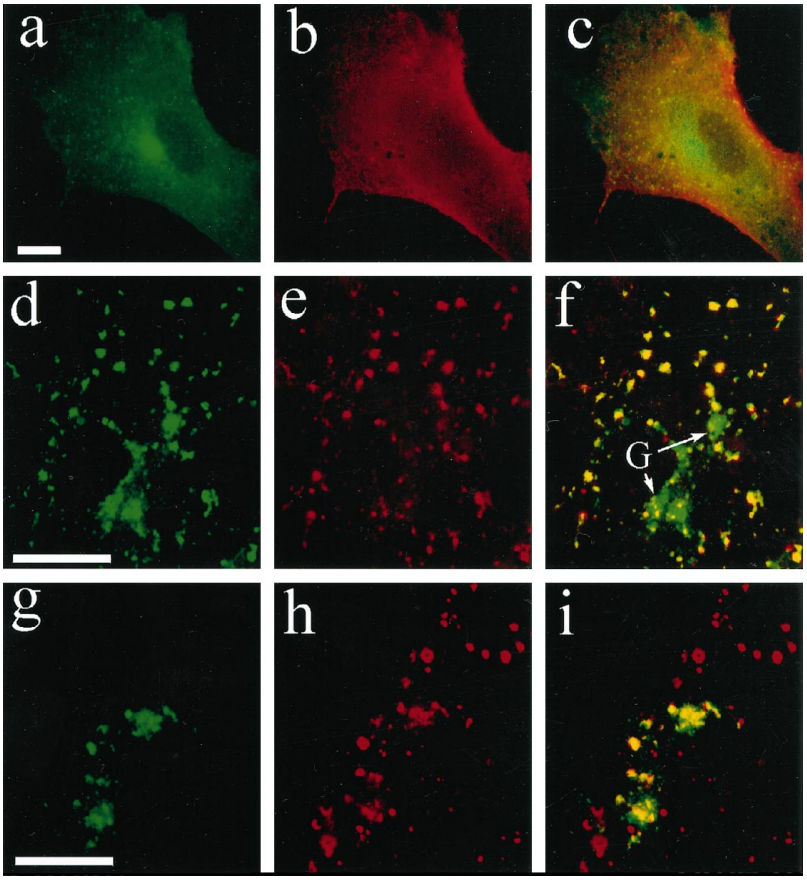

FIG. 8. **Co-localization of EGF-TR and EGFR-GFP during endocytosis in living cells.** PAE cells (clone A11) expressing EGFR-GFP were grown in microscope chambers and serum-starved overnight. EGF-TR (20 ng/ml) was added to the chamber, and the living cell images of Texas Red and GFP fluorescence were acquired after 1 min of incubation. After 5 min of continuous incubation, the medium was changed to a fresh binding medium without EGF-TR, and the cells were further incubated at 37 °C. The stacks of 200-nm optical sections of GFP (*d* and *g*) and Texas Red fluorescence (*e* and *h*) were acquired after 30 (*d–f*) and 70 min (*g–i*) of the chase incubation using QED Imaging workstation and deconvoluted on a Deltavision workstation. Binning 2 × 2 was used to increase the sensitivity of the camera. Exposure time was 0.3 s per section. The optical sections through the middle of the cell corresponding to the best focus on perinuclear endosomes are presented in *d–i*. Co-localization is shown by the overlap of *green* (EGFR-GFP) and *red* fluorescence (EGF-TR) resulting in *yellow* staining. EGFR-GFP located in Golgi area ("*G*") and not co-localized with EGF-TR is indicated. *Bars*, 5 μm.

EGF-TR and EGFR-GFP are seen co-localized in the same vesicular structures, likely endosomes, after 30 min of chase incubation. The endosomal compartments were rapidly moving and often had a complex morphology consisting of a vesicular portion and tubular extensions. In addition, diffuse GFP staining at the periphery of the cell and accumulation of GFP in the Golgi region are seen, which presumably correspond to the surface receptors and newly synthesized receptors on the way to the surface, respectively. At the late stages of intracellular trafficking, EGFR-GFP and some EGF-TR remain co-localized in the large perinuclear endosomes, probably, MVEs (Fig. 8, *g–i*). However, a significant fluorescence of Texas Red is associated with the peripheral vesicular compartments that do not contain GFP. It is possible that EGF-TR dissociates at the late stages of endocytosis from the EGFR-GFP and is accumulated in lysosomes. Another possibility is that the entire EGF-TR·EGFR-GFP complex is sorted to lysosomes where GFP is destroyed faster than Texas Red. In fact, Texas Red remains visible in cells that were allowed to endocytose EGF-TR for 1 h and were chased overnight in medium without EGF-TR (data not shown).

Low-light real-time microscopy allows monitoring of the rapid dynamics of EGFR-GFP trafficking during the early stages of receptor endocytosis. PAE cells stimulated with unlabeled EGF were continuously observed by time-lapse digital microscopy. As expected EGFR-GFP is seen in small vesicles that are seen to move very rapidly often migrating toward a perinuclear area. In addition, the presence of EGFR-GFP in the large endosomal compartments consisting of the vesicular swellings ("varicosities," see Ref. 11) and thin tubular extensions is observed. Fig. 9 presents several images from a small region of a single cell acquired between the 2nd and the 5th min after EGF addition. Analysis of these images demonstrates the dynamic behavior of a tubular-vesicular endosome and the direct visualization of a fusion event. The example in Fig. 9 shows a flickering behavior of a small varicosity that encounters a relatively stationary large swelling (*frame 55*) but does not initially fuse with it and moves away along the tubule (*frames 56* and *62*). Then the small vesicle moves toward the large compartment again and fuses with it (*frames 91–179*). The large network of vesicles including the small and large varicosities connected by a tubular structure is clearly seen in *frame 197*. In addition to this fusion event, the large varicosity has increased in size due to assimilation of a very small vesicle between *frames 15* and *55* (data not shown). Other vesicles within the area are also changing position and moving during the time course experiment. Thus real-time fluorescence microscopy of living cells allows visualization of the rapid dynamics of EGFR-GFP within the tubular-vesicular endosomal networks that are not preserved in chemically fixed cells.

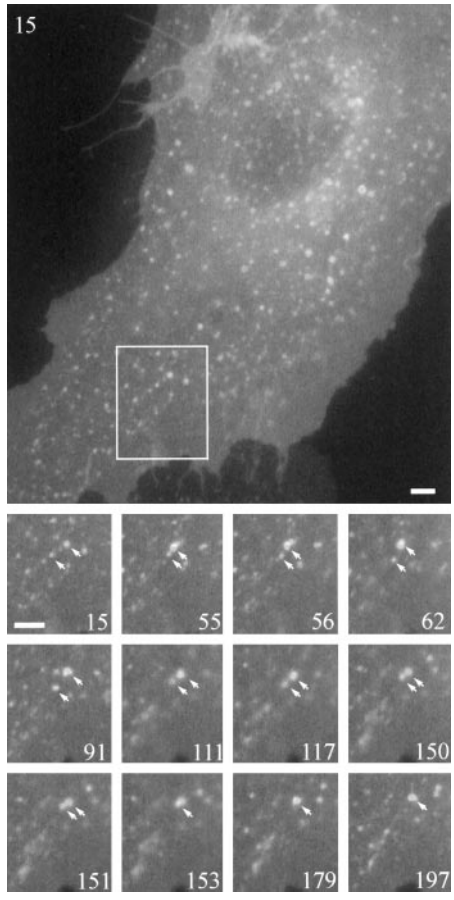

FIG. 9. **Dynamics of EGFR-GFP-containing endosomes in living cells.** PAE cells (clone A11) expressing EGFR-GFP were grown on microscope chambers and serum-starved overnight. EGF (50 ng/ml) was added to the chamber, and time-lapse image acquisition of GFP fluorescence was performed at 37 °C. Images were acquired 2 times per s with the exposure time of 0.3 s and a 5% light intensity of the mercury light source. Presented are the selected images taken between the 2nd and 5th min after EGF addition. The *large top panel* shows the 15th frame, whereas high magnification time-lapse images of a selected region of the cell (*white box*) are indicated by the number of the image. Binning 2 × 2 was used to increase the sensitivity of the camera. *Arrows* highlight the movement and ultimate fusion of the two EGFR-GFP-containing vesicular portions of a large tubular-vesicular endosomal compartment that is clearly visible in *frame 197*. *Bar*, 1 μm. The full version of a time-lapse movie can be viewed at http://porsche.uchsc.edu/pharm/faculty/sorkin.index.htm.

DISCUSSION

Advances in the development of proteins conjugated with GFP provide the opportunity for real-time optical analysis of protein trafficking in individual cells. Here we describe the characterization of the first GFP chimera of a receptor tyrosine kinase, EGFR-GFP, in which the GFP moiety is attached to the carboxyl terminus of the receptor. The fusion of GFP to the cytoplasmic tail of EGFR could be expected to interfere with the receptor function because the carboxyl-terminal domain regulates kinase activity and receptor interactions with other proteins. On the other hand, placement of the GFP tag at the amino terminus would possibly hinder the translocation and processing of newly synthesized EGFR and ligand binding. The simplicity of cloning and the convenience in using it for mutagenesis and for conversion to other color fluorescent protein chimeras determined our strategy of fusion at the carboxyl terminus.

Surprisingly, characterization of the EGFR-GFP chimera shows that it behaves essentially unperturbed in its cellular and biochemical properties when compared with EGFR-wt. EGFR-GFP is activated normally by EGF as judged by receptor autophosphorylation, tyrosine kinase activity *in vivo,* and activation of MAP kinase pathway. Certainly, EGF may trigger other signal transduction pathways, and we cannot rule out that the future analyses may uncover a defect in one of these pathways in EGFR-GFP-expressing cells. Interestingly, neither phosphorylation of major *in vivo* sites, tyrosines 1148 and 1173 (27), nor binding of Shc to these tyrosines is affected by the fusion of GFP in close proximity (residue 1186) to these residues. Apparently, the attachment of a 26-kDa protein does not constrain EGF-induced conformational rearrangements of the rest of the receptor molecule.

The kinetics of internalization and postendocytic trafficking of EGFR-GFP appear to be essentially similar to that of native EGFR. In NIH 3T3 or PAE cells, the chimera traffics at a rate similar to that measured for EGFR-wt expressed in these cells

and for endogenous receptors in other cells. In contrast, HEK 293 cells do not have the capacity to rapidly endocytose and down-regulate overexpressed EGFR-GFP or EGFR-wt, even when very small numbers of EGFR are activated by low concentrations of EGF. These data suggest that the large excess of unoccupied EGFR can compete with activated EGFR for internalization leading to the saturation of the pathway and that the mechanisms that regulate the capacity of the EGFR internalization machinery are cell-specific.

Interestingly, the products of partial proteolysis of the extracellular domain of EGFR-GFP could be detected in EGF-treated cells (Figs. 2 and 3), whereas such forms of native EGFR have not been previously identified (20, 28, 29). It is possible that GFP sterically hinders the normal rapid degradation of the receptor cytoplasmic domain to small peptides, which allows the products of partial degradation to accumulate to detectable levels. The truncated forms are not immunoprecipitated by the antibodies specific to the EGFR extracellular domain (Fig. 5 and Refs. 20 and 28). Furthermore, the sensitivity of EGFR detection by most specific antibodies depends on the phosphorylation status of the carboxyl terminus. In contrast, the recognition of the chimera by anti-GFP is very sensitive and does not depend on the state of the receptor. Thus, EGFR-GFP might be useful for biochemical analyses of the receptor function.

Fluorescent receptor ligands, EGF-TR, and anti-EGFR antibodies have been previously used to follow the endocytosis of EGFR in living cells (11, 16). We took advantage of the GFP fluorescence to simultaneously follow the localization of both EGF and EGFR in living cell. It was found that EGF-TR and EGFR-GFP are mainly localized in the same compartments during the early stages of endocytosis but become segregated at later stages. The co-localization of EGF-TR and EGFR-GFP was more prolonged when EGF-TR was continuously present (data not shown). These observations are consistent with the hypothesis that the bulk of EGF-EGFR complexes remain intact in early endosomes and MVE (30–32). The segregation of EGF-TR from the receptor during pulse-chase experiments suggests that the applicability of EGF-TR as a marker of EGFR trafficking is limited to the analysis of the early events of EGFR endocytosis and that directly labeled EGFR can be a powerful tool to study ligand-independent receptor trafficking.

Studies of endocytosis of fluorochrome-labeled transferrin using living cell microscopy identified the endosomal compartment as an extensive network of tubular membranes (11). In a later study, the fluorescent antibody to EGFR was located in discrete swellings of this tubular reticulum. The sorting of the endocytic markers, such as EGFR, to the vesicular compartments is thought to be the mechanism of the lysosomal targeting (33). Our experiments with EGFR-GFP in living cells demonstrate that EGFR is present in both the tubular and the vesicular sub-domains of the endosomes. This is in agreement with the observation of efficient recycling of EGF-receptor complexes from early endosomes (13).

Two types of dynamic motility of EGFR-GFP-containing organelles were observed. First, rapid movement of the apparently separated vesicles toward the perinuclear area is frequently seen. This endosomal movement is presumably microtubular-dependent and is described previously in several studies (34, 35). A slower flickering of varicosities along endosomal tubules and the fusion of small varicosities with the bigger and more stationary vesicular compartments within the tubular-vesicular endosomes was also observed (Fig. 9). The flickering behavior of endosomal membranes is consistent with the existence of the biochemical mechanisms that tightly control the timing of the endosomal fusion (36). Collectively, the data suggest that both the lateral movement of endocytic markers within the maturing endocytic compartments and the transport and selective vesicle fusion events occur at the early stages of endocytosis. The example of endosomal dynamics presented in Fig. 9 shows that the large endosomes, probably MVEs, form by consecutive assimilation of several small varicosities.

Here, we demonstrate that direct visualization of EGF-GFP distribution circumvents the limitations conferred by fixation and permeabilization allowing visualization of fragile endosomal compartments. The availability of other variants of GFP with distinct spectral properties suggest that it may be possible to probe the kinetics of the interaction of the EGFR with adaptor and effector molecules in real time *in vivo*. Fluorescence resonance energy transfer studies with EGFR-GFP and multicolor GFP-labeled proteins are in progress in our laboratory.

Acknowledgments—We thank Drs. Ashley Davis and Fransesc Tebar for critically reading the manuscript. We are grateful to Drs. Carpenter and Beguinot for the gift of antibodies.

REFERENCES

1. Carpenter, G., and Cohen, S. (1976) *J. Cell Biol.* **71,** 159–171
2. Beguinot, L., Lyall, R. M., Willingham, M. C., and Pastan, I. (1984) *Proc. Natl. Acad. Sci. U. S. A.* **81,** 2384–2388
3. Sorkin, A., and Waters, C. M. (1993) *BioEssays* **15,** 375–382
4. Sorkin, A., and Carpenter, G. (1993) *Science* **261,** 612–615
5. Boll, W., Gallusser, A., and Kirchhausen, T. (1995) *Curr. Biol.* **5,** 1168–1178
6. Nesterov, A., Kurten, R. C., and Gill, G. N. (1995) *J. Biol. Chem.* **270,** 6320–6327
7. Nesterov, A., Wiley, H. S., and Gill, G. N. (1995) *Proc. Natl. Acad. Sci. U. S. A.* **92,** 8719–8723
8. Sorkin, A., Mazzotti, M., Sorkina, T., Scotto, L., and Beguinot, L. (1996) *J. Biol. Chem.* **271,** 13377–13384
9. Hopkins, C. R., Miller, K., and Beardmore, J. M. (1985) *J. Cell Sci.* **3,** (suppl.) 173–186
10. Miller, K., Beardmore, J., Kanety, H., Schlessinger, J., and Hopkins, C. R. (1986) *J. Cell Biol.* **102,** 500–509
11. Hopkins, C. R., Gibson, A., Shipman, M., and Miller, K. (1990) *Nature* **346,** 335–339
12. Hopkins, C. R., and Trowbridge, I. S. (1983) *J. Cell Biol.* **97,** 508–521
13. Sorkin, A., Krolenko, S., Kudrjavtceva, N., Lazebnik, J., Teslensko, L., Soderquist, A. M., and Nikolsky, N. (1991) *J. Cell Biol.* **112,** 55–63
14. Felder, S., Miller, K., Moehren, G., Ullrich, A., Schlessinger, J., and Hopkins, C. R. (1990) *Cell* **61,** 623–634
15. Futter, C. E., Pearse, A., Hewlett, L. J., and Hopkins, C. R. (1996) *J. Cell Biol.* **132,** 1011–1024
16. Schlessinger, J., Shechter, Y., Willingham, M. C., and Pastan, I. (1978) *Proc. Natl. Acad. Sci. U. S. A.* **75,** 2659–2663
17. Chalfie, M., Tu, Y., Euskirchen, G., Ward, W. W., and Prasher, D. C. (1994) *Science* **263,** 802–805
18. Barak, L. S., Ferguson, S. S. G., Zhang, J., Martenson, C., Meyer, T., and Caron, M. G. (1997) *Mol. Pharmacol.* **51,** 177–184
19. Kallal, L., Gagnon, A. W., Penn, R. B., and Benovic, J. L. (1998) *J. Biol. Chem.* **273,** 322–328
20. Sorkin, A., Waters, C. M., Overholser, K. A., and Carpenter, G. (1991) *J. Biol. Chem.* **266,** 8355–8362
21. Bertics, P. J., Weber, W., Cochet, C., and Gill, G. N. (1985) *J. Cell. Biochem.* **29,** 195–208
22. Tebar, F., Sorkina, T., Sorkin, A., Ericsson, M., and Kirchhausen, T. (1996) *J. Biol. Chem.* **271,** 28727–28730
23. Rossomando, A. J., Payne, D. M., Webber, M. J., and Sturgill, T. W. (1989) *Proc. Natl. Acad. Sci. U. S. A.* **86,** 6940–6943
24. Pelicci, G., Lafrancone, L., Grignane, F., McGlade, J., Cavallo, F., Forni, G., Nicoletti, N., Grignani, F., Pawson, T., and Pelicci, P. G. (1992) *Cell* **70,** 93–103
25. Soler, C., Beguinot, L., and Carpenter, G. (1994) *J. Biol. Chem.* **269,** 12320–12324
26. Sorkin, A., Westermark, B., Heldin, C.-H., and Claesson-Welsh, L. (1991) *J. Cell Biol.* **112,** 469–478
27. Bertics, P. J., Chen, W., Hubler, L., Lazar, C. S., Rosenfeld, M. G., and Gill, G. N. (1988) *J. Biol. Chem.* **263,** 3610–3617
28. Stoscheck, C. M., and Carpenter, G. (1984) *J. Cell Physiol.* **120,** 296–302
29. Wiley, H. S., Herbst, J. J., Walsh, B. J., Lauffenberger, D. A., Rosenfeld, M. G., and Gill, G. N. (1991) *J. Biol. Chem.* **266,** 11083–11094
30. Sorkin, A., Teslenko, L., and Nikolsky, N. (1988) *Exp. Cell Res.* **175,** 192–205
31. Lai, W. H., Cameron, P. H., Doherty, J.-J., II, Posner, B. I., and Bergeron, J. J. M. (1989) *J. Cell Biol.* **109,** 2751–2750
32. Sorkin, A., and Carpenter, G. (1991) *J. Biol. Chem.* **266,** 23453–23460
33. Hopkins, C. R. (1992) *Trends Biochem. Sci.* **17,** 27–32
34. de Brabander, M., Nuedens, R., Geerts, H., and Hopkins, C. R. (1988) *Cell Motil. Cytoskel.* **9,** 30–47
35. Aniento, F., Emans, N., Griffiths, G., and Gruenberg, J. (1994) *J. Cell Biol.* **123,** 1373–1387
36. Rybin, V., Ullrich, O., Rubino, M., Alexandrov, K., Simon, I., Seabra, C., Goody, R., and Zerial, M. (1996) *Nature* **383,** 266–269